

## Article

# Prediction of the Remaining Useful Life of Lithium-Ion Batteries Based on the 1D CNN-BLSTM Neural Network

Jianhui Mou <sup>1</sup>, Qingxin Yang <sup>1</sup>, Yi Tang <sup>1,\*</sup>, Yuhui Liu <sup>2</sup>, Junjie Li <sup>1</sup> and Chengcheng Yu <sup>1</sup>

<sup>1</sup> School of Electromechanical and Automotive Engineering, Yantai University, Yantai 264005, China; mujianhui@ytu.edu.cn (J.M.); yangqx0831@s.ytu.edu.cn (Q.Y.); lijunjie@ytu.edu.cn (J.L.); ycc970118@s.ytu.edu.cn (C.Y.)

<sup>2</sup> Suzhou Tongyuan Software & Control Technology Co., Ltd., Suzhou 215125, China

\* Correspondence: tangyi0319@126.com

**Abstract:** Lithium-ion batteries are currently widely employed in a variety of applications. Precise estimation of the remaining useful life (RUL) of lithium-ion batteries holds significant function in intelligent battery management systems (BMS). Therefore, in order to increase the fidelity and stabilization of predicting the RUL of lithium-ion batteries, in this paper, an innovative strategy for RUL prediction is proposed by integrating a one-dimensional convolutional neural network (1D CNN) and a bilayer long short-term memory (BLSTM) neural network. Feature extraction is carried out through the input capacity data of the model using 1D CNN, and these deep features are used as the input of the BLSTM. The memory function of the BLSTM is applied to retain key information in the database and to better understand the coupling relationship among consecutive time series data along the time axis, thereby effectively predicting the RUL trends of lithium-ion batteries. Two different types of lithium-ion battery datasets from NASA and CALCE were used to verify the effectiveness of the proposed method. The results show that the proposed method achieves higher prediction accuracy, demonstrates stronger generalization capabilities, and effectively reduces prediction errors compared to other methods.



**Citation:** Mou, J.; Yang, Q.; Tang, Y.; Liu, Y.; Li, J.; Yu, C. Prediction of the Remaining Useful Life of Lithium-Ion Batteries Based on the 1D CNN-BLSTM Neural Network. *Batteries* **2024**, *10*, 152. <https://doi.org/10.3390/batteries10050152>

Academic Editors: Carlos Ziebert and Pascal Venet

Received: 13 February 2024

Revised: 13 April 2024

Accepted: 24 April 2024

Published: 30 April 2024



**Copyright:** © 2024 by the authors. Licensee MDPI, Basel, Switzerland. This article is an open access article distributed under the terms and conditions of the Creative Commons Attribution (CC BY) license (<https://creativecommons.org/licenses/by/4.0/>).

**Keywords:** prediction of RUL; lithium-ion batteries; 1D CNN; BLSTM; hybrid method

## 1. Introduction

The application of energy storage technologies brings fresh chances and challenges for the renewable energy revolution. The lithium-ion battery has been one of the rapid developing electrochemical energy storage technologies in recent years owing to its high energy density, environmental protection and long lifetime, and other advantages [1,2]. Its applications span across various fields, including military, aerospace, and electronic products. The swift advancement of emerging technologies heavily relies on the critical role played by lithium-ion batteries, such as information technology, renewable energy sources, and environmental conservation. Meanwhile, lithium-ion batteries also have security and dependability hazards, including overcharging, overdischarging, overheating, and differences in single-cell lifespan. Remaining useful life (RUL) prediction is the fundamental technology for managing the health of lithium-ion batteries, serving as a vital approach to grasp the declining trend in power performance. Consequently, the RUL prediction of lithium-ion batteries has been receiving concentration in recent years [3–5]. Accurately predicting the RUL is crucial for ensuring the reliable operation of batteries throughout their entire energy storage lifespan. The capacity is broadly regarded as a sign of health, which is used to evaluate the remaining cycle life of a battery [6,7]. Lithium-ion batteries are dynamic and ever-changing electrochemical systems with nonlinear characteristics and complex internal mechanisms, which exposes great challenges for predicting maximum remaining capacity and minimizing the declining trend.

Based on the literature investigation, the prediction of lithium-ion battery RUL is primarily classified into model-based methods, data-driven methods, and hybrid methods [8].

### (1) The model-based method

The model-based method describes the aging behavior of batteries through mathematical and physical models. This approach typically consists of a range of algebraic or differential equations, whose most essential features are tailored to a specific system. Model-based RUL prediction methods can be constructed using electrochemical models (EM) [9], equivalent circuit models (ECM) [10], or empirical models [11]. EM relies on capturing the internal characteristics of the battery to describe the physical processes of the electrochemical system. Wang investigated the relationship between solid electrolyte thin films and capacity degradation, and developed a single-particle model to simulate the degradation process of batteries [12]. Singh developed a semi-empirical model for the discharge curve of lithium-ion batteries to determine the maximal storage capacity after every charge–discharge cycle [13]. Such models establish empirical correlation between the model parameters, just limited to specific battery systems. Zhang developed an RUL prediction approach for lithium-ion batteries, which combines the exponential model and particle filter. This approach is specifically designed to tackle the challenges posed by the batteries' nonlinear and non-gaussian capacity regression features [14]. Lyu et al. introduced a novel particle filter framework to predict the RUL of lead-acid batteries. This method integrates the battery's electrochemical models, enhancing the precision and dependability of RUL prediction. The parameters of the model describing battery decline were viewed as state variables inside the framework [15]. The EM based RUL prediction of lithium-ion batteries allows for an exhaustive description of the inside physical and chemical reactions of the battery as it ages, starting from the battery degradation mechanism. However, the EM requires the application of a huge number of thermodynamic and kinetic equations, which involve a large number of parameters and variables, as well as complex computational processes that make it harder to thoroughly account for all environmental and service-related factors. Therefore, the prediction of RUL based on EM has the problem of modeling difficulty. Hu assessed the complexity, correctness, and robustness of twelve equivalent circuit models [16]. Though ECM have fewer parameters, parameter identification is relatively simple and the state space equation is easily available compared to for the EM. However, owing to the complicated inside structure of lithium-ion batteries and the dynamic nature of the internal parameters during operation, it is very difficult to establish a suitable ECM, and to take into account the intricate external conditions, which makes the ECM has poor generality relatively. Therefore, the model-based RUL prediction method has the problems of modeling difficulties and practical application difficulties.

### (2) The data-driven method

Contrasted with model-based methods, data-driven methods take no account of the complex electrochemical reactions and ageing mechanisms within lithium-ion batteries, and instead place emphasis on the battery performance test and operational status data that can be monitored and obtained, exploring the battery performance information and evolution patterns hidden in these data. The data-driven method begins with feature extraction by leveraging and analyzing large amounts of raw data, and then applying specific algorithms to predict battery health. Data-driven methods currently cover the artificial neural networks (ANNs) [17,18], related vector machines (RVM) [19], support vector machines (SVM) [20], gaussian process regression (GPR), long short-term memory (LSTM) [21,22], etc. Richardson proposed a gaussian process (GP) regression for predicting the RUL of batteries, and data-driven methods demonstrate excellent predictive capabilities for long short-term prediction of RUL [23]. In addition to an iterative multi-step prediction model based on support vector regression (SVR), Wang also developed a non-iterative prediction model based on flexible support vector regression (F-SVR) by inputting low-dimensional battery external characteristics data to acquire better RUL prediction results

for lithium-ion batteries [24]. Song employed a RVM for RUL prediction, which demonstrated the excellent short-term prediction ability. The study introduces an innovative iterative update approach aimed at enhancing the long-term prediction ability [25]. The literature [26,27] successfully predicted the capacity of a single battery using a mixture of back-propagation (BP) neural networks and an extended Kalman filter. For battery capacity calculation and RUL prediction, Rezvani et al. utilized both the linear prediction error method (L-PEM) and the adaptive neural network (AdNN) [28]. They discovered that AdNN gave a greater precise one-step forward capacity prediction, whereas L-PEM demonstrated a more accurate prediction of RUL. In [29], the recurrent neural network (RNN) approach is utilized to predict the condition of healthy batteries, without iteration and feature extraction to predict the attenuation trend at one time. Because during the initial aging process, the capacity degradation of the battery usually does not happen right away, it is crucial to extract the aging characteristics in order to predict the RUL of lithium-ion batteries before the capacity is significantly decreased. Once suitable features have been extracted, deep learning can realize effective prediction. As an RNN variation, Long Short-Term Memory (LSTM) has been specifically designed to tackle the issues of vanishing or exploding gradients during the training phase, leading to substantial improvements in its gradient management capabilities. Li achieved the compelling results by employing the LSTM to predict the RUL of lithium-ion batteries [30]. However, RNN and LSTM models are prone to underfitting issues when the measured values are noisy or there are insufficient amounts of data. CNN have demonstrated the capability to effectively address the underfitting problem, proving particularly valuable when dealing with noisy measurements or limited quantities of data. Generally, the data-driven approach predicts future capacity decay trends from historical degradation data through specific algorithms without the need to build complex mathematical or physical models, making it well suited for practical application in real-world working environments. To improve parameter determination, confidence intervals, and long-term prediction performance, this method is employed in conjunction with other types of optimization algorithms.

### (3) The hybrid method

Hybrid methods have gained increasing prominence in the research sector in recent years. The fusion of multiple algorithms is conducive to conquer the limitations of a single algorithm and give full leverage for the strengths of different algorithms, in order to acquire better prediction results. Currently, the hybrid method for RUL prediction is classified into two types—model hybrid and data hybrid. By combining the regularized particle filter algorithm and the nonlinear degradation-autoregressive model, Song proposed a unique method for lithium-ion battery RUL prediction [31]. Mo developed the Kalman filter combined with standard particle filtering and particle swarm optimization for RUL estimation of lithium-ion battery with excellent accuracy [32]. Xue introduced an integrated algorithm that combines the adaptive unscented Kalman filter (AUKF) with genetic algorithm-optimized support vector regression (GA-SVR) to achieve multi-step prediction of lithium-ion battery RUL. The proposed AUKF-GA-SVR approach demonstrates improved prediction accuracy [33]. Song created a fusion RUL prediction approach by integrating RVM and KF. Due to RVM's excellent performance of short-term prediction and poor performance of long-term prediction, an iterative updating method was presented to enhance the long-term prediction performance of lithium-ion battery RUL prediction [25]. Cao proposed time series prediction models that incorporate two types of empirical mode decomposition (EMD) and the LSTM. Experimental findings demonstrate that the suggested approaches outperform others in one-step-ahead financial time series prediction [34]. Qu proposed an LSTM-based wind prediction model. The results of simulation indicate that the LSTM model outperforms the SVM model and the BP neural network in prediction accuracy [35]. Inspired by the data hybrid method, this paper presented the CNN-BLSTM, an innovative hybrid neural network for predicting the RUL of lithium-ion batteries. The CNN-BLSTM fully utilizes CNN's feature extraction ability as well as BLSTM's time series prediction ability to achieve reliable prediction, which may significantly enhance the RUL

estimate performance of lithium-ion batteries. The different prediction methods for RUL are summarized in Table 1.

**Table 1.** Summary of different RUL estimation methods.

Methods	Advantages	Disadvantages
Model based	The growth trend of internal resistance can be effectively described	Difficult to establish or identify model parameters
Data driven	Wide range of applications and high precision	Requires a large amount of data training and lacks sparsity and parameter sensitivity
Hybrid methods	High precision and strong generalization ability	Strong data dependency and requiring a large amount of computation

This research contributes to the field in the following ways.

1. Broad applicability and excellent precision. The suggested method is evaluated using two different battery types, achieving superior accuracy compared to other regularly used methods.
2. The hybrid model CNN-BLSTM is formed by integrating fundamental neural network, CNN and LSTM, utilizes a single-channel (i.e., capacity) approach to reliably predict the RUL of lithium-ion batteries. This hybrid neural network comprises one convolutional layer and two LSTM layers, forming an end-to-end framework for both model training and RUL prediction.
3. This study offers comprehensive insights into single and hybrid methods for RUL prediction in lithium-ion batteries through a comparative analysis of BP, CNN, LSTM, BLSTM, and CNN-LSTM. The CNN-BLSTM method surpasses these comparable methods in RUL estimation results.

The following is an outline of this paper's content. Section 2 discusses the research in this paper and develops a specific discussion of state of health (SOH) and RUL for lithium-ion batteries. Section 3 describes the CNN, LSTM, and BLSTM algorithms and related fusion algorithms. Section 4 validates and analyzes the suggested algorithm's prediction outcomes and compares them to the other algorithms. Section 5 draws the conclusion.

## 2. Research Object and Content

Although the fact that lithium-ion batteries offer great energy density, reusability and low self-discharge rate, during the battery charging and discharging process, irreversible physicochemical reactions occur in the materials inside the battery such as the electrolyte, and these reactions will eventually lead to a decrease in battery performance. The basic principle of lithium-ion batteries relies on the process of intercalation and de-intercalation of lithium ions between the positive and negative electrodes. These processes constitute the battery's charge and discharge cycle, allowing electrical energy to be reversed between positive and negative electrodes.

SOH is a health indicator that depicts the battery's aging status during every charge-discharge cycle. Parameters such as capacity, internal resistance, electric quantity, and peak power are frequently utilized as indicators to represent SOH [36]. The ratio of the lithium-ion battery capacity at the current moment to the initial battery capacity is chosen as the SOH definition norm, and the SOH in the  $k - th$  cycle can be defined by the formula below.

$$SOH(k) = \frac{C_k}{C_o} \times 100\% \quad (1)$$

where  $C_o$  is the lithium-ion battery's rated capacity, respectively;  $C_k$  is the capacity of the lithium-ion battery at the  $k - th$  full charge.

A battery's RUL reflects the count of effective charge-discharge cycles remaining at a given point in its cycle. A battery cycle is defined as a full charge-discharge cycle, and the cycle count refers to the method of calculating the number of such charge-discharge

cycles. Since the battery completes one full charge and discharge cycle, the cycle count increases by one. The lithium-ion battery is deemed to be at the end of life (EOL) when the battery actual capacity decays to the failure threshold. The capacity value of battery failure is known as the EOL threshold, and it is usually regarded as the capacity to reach 70~80% of the nominal capacity. Therefore, a battery's RUL is defined as follows.

$$T_{RUL} = T_{EOL} - T \quad (2)$$

where  $T$  represents the cycle amount at the present capacity, while  $T_{EOL}$  denotes the cycle amount at the EOL threshold.

The SOH and RUL express several elements of battery state. The SOH quantitatively describes the current performance state of the battery by comparing it to its initial state, while the RUL indicates the reliable estimate of the number of remaining valid cycles between now and the future.

### 3. The Hybrid Neural Network

#### 3.1. The Convolution Neural Network (CNN)

CNN is a feedforward neural network with a deep structure. It is specifically designed to process data with a network structure [37]. The CNN executes convolutional operations on local area capacity data to extract the information features of higher dimensions between the input information. Therefore, CNN possesses the characteristic of effectively extracting the deep features of capacity data. CNN consists of 3D, 2D, and 1D CNNs, with the following distinctions:

- By incorporating the time dimension into the 3D CNN input, the neural network can concurrently capture both temporal and spatial features, enabling effective video processing and behavior identification.
- The 2D CNN is mainly used to process two-dimensional data and is widely used in image recognition and computer vision. In video processing, the spatial position information of each pixel is represented in two dimensions, typically width and height. As a result, 2D CNNs can effectively capture the spatial features and structures in the image.
- The 1D CNN is mainly used to process one-dimensional sequence data, and is commonly used in time series analysis and natural language processing such as text classification, sentiment analysis, and signal processing. In time series data, information is typically represented in a single dimension time or location in a series. The 1D CNN is suitable for extracting local features and patterns from sequence data.

Because the battery capacity is based on one-dimensional data of the time series, 1D CNN is more appropriate for predicting lithium-ion battery capacity decay.

The 1D CNN structure involves an input layer, a convolutional layer, a pooling layer, and an output layer, as seen in Figure 1. The convolutional layer executes convolution operations on the input data throughout the CNN model's learning phase, generating abstract features containing spatial information that serve as input for the next layer. The pooling layer executes localized data processing on the output from the convolutional layer to accomplish data feature extraction and information screening. The fully connected layer is located at the last layer of the CNN, where neurons are connected with weighted connections to all neurons in the previous layer. After the input samples undergo multiple layers of processing, including the convolutional layer and pooling layer, the input samples are eventually merged and compacted through the fully connected layer, the excitation function is applied for the ultimate categorization or regression examination of the input samples.

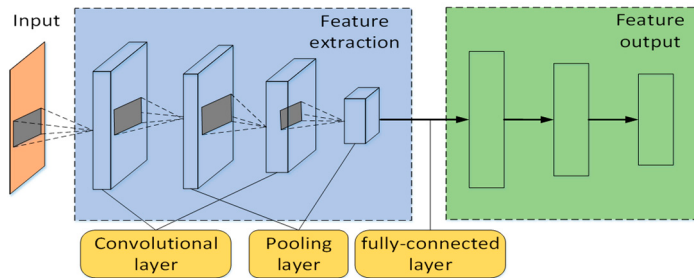


**Figure 1.** Schematic diagram of the 1D CNN structure.

The input data conducts convolutional operation in the one-dimensional convolutional layer, as shown in Equation (3).

$$x_t^l = \sum_{i=1}^{N_{l-1}} conv1D(w_{it}^{l-1}, s_i^{l-1}) + b_t^l \quad (3)$$

where  $x_t^l$  and  $b_t^l$  represent the input and bias of the neuron,  $w_{it}^{l-1}$  represents the neural node's convolution kernel,  $s_i^{l-1}$  represents the neural node's output,  $N_{l-1}$  represents the number of neural nodes, and  $conv1D$  represents 1D convolution operation.

To enhance the nonlinear learning capability of the fusion neural network, the rectified linear (*ReLU*) activation function is used in the convolution process of lithium-ion battery capacity data, as demonstrated by Equation (4). The utilization of the *ReLU* function can accelerate the training and enhance the network's training stability. To some extent, it can address the issue of vanishing gradients and expedite the convergence speed of gradient descent.

$$\text{ReLU}(x) = \max(0, x) \quad (4)$$

Because the pooling layer only features extraction and does not contain training parameters, it reduces the neural network parameters and effectively mitigates overfitting, thus improving the generalization capability of the network. This can be described as.

$$s_t^l = \max_{(t-1)H+1 \leq j \leq tH} (s_j^{l-1}) \quad (5)$$

In Equation (5),  $s_t^l$  denotes the pooling function's output.

### 3.2. Bilayer Long and Short-Term Memory (B-LSTM) Network

#### 3.2.1. Long and Short-Term Memory (LSTM) Network

The LSTM network is a variant of recurrent neural network (RNN), mainly used to effectively solve the challenges of vanishing gradients and gradient explosion in the RNN [38,39]. By preserving valuable information and discarding irrelevant data, the learning processing is simplified. The network accomplishes memory state writing, reading, and deletion by introducing a storage state and several gating units [34]. LSTM is widely applied in various domains, including speech recognition, machine translation, and handwriting recognition.

Figure 2 depicts the internal structure of LSTM. Compared with the RNN structure, LSTM introduces an input gate  $i_t$ , a forget gate  $f_t$ , an output gate  $o_t$ , and a memory cell  $C_t$ . These gates are used to update or discard historical information and avoid the gradient disappearance problem triggered by the gradient back-propagation over time in a specific way, thus giving the LSTM a long-term memory function [40,41]. The LSTM hidden layer utilizes input vector  $x_t$  and output vector  $h_t$  to implement the activation function and weight updates. The principle formula for the LSTM cell is.

$$i_t = \sigma(W_i \cdot x_t + U_i \cdot h_{t-1} + b_i) \quad (6)$$

$$f_t = \sigma(W_f \cdot x_t + U_f \cdot h_{t-1} + b_f) \quad (7)$$

$$\tilde{C}_t = \tanh(W_c \cdot x_t + U_c \cdot h_{t-1} + b_c) \quad (8)$$

$$C_t = f_t * C_{t-1} + i_t * \tilde{C}_t \quad (9)$$

$$o_t = \sigma(W_o \cdot x_t + U_o \cdot h_{t-1} + b_o) \quad (10)$$

$$h_t = o_t * \tanh C_t \quad (11)$$

where  $\tanh$  is the hyperbolic tangent activation function.  $\tilde{C}_t$  is the intermediate result obtained by applying the function  $\tanh$  to the input information and past information.  $\sigma$  is the sigmoid function.  $*$  is the Hadamard product.  $W$  and  $U$  are the weight matrix.  $b$  is the bias term.

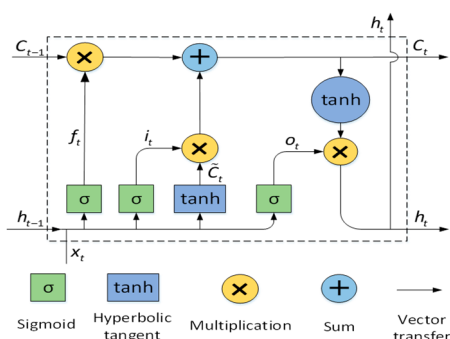


**Figure 2.** Diagram of LSTM unit.

### 3.2.2. The Operating Principle of BLSTM

As an upgraded version of the LSTM network algorithm, BLSTM trains and learns the data processed by the CNN layer, deeply extracts the dependency relationship between capacity and charge discharge cycle period, and has a memory function. The BLSTM structure installs two layers with a similar construction and operation principle to the hidden layer, namely the lower and the upper LSTM hidden layer, as seen in Figure 3. The lower and upper LSTM layer, respectively, conduct feature retrieval and knowledge storage of the input sequence's context. The ultimate end output consequence of the BLSTM network can be derived through the combination of the lower layer and upper layer output values. Compared with single-layer LSTM network processing input data, the lower layer of BLSTM can extract the dependency between the battery capacity and the hidden quantity of battery charging and discharging cycles, while the upper layer captures the deeper dependency between the two. The hidden state  $h_t^1$  of the lower layer is completely connected to the hidden state  $h_t^2$  of the upper layer. Finally, the output of the hidden state of the upper layer can be obtained. The update process of the BLSTM is represented by the Equation (12).

$$h_t^2 = W_m \cdot h_t^1 + b_m \quad (12)$$

where  $W_m$  and  $b_m$  are the network fully connected weight matrix and bias vector between the lower layer LSTM and upper layer LSTM, respectively;  $h_t^1$  denotes the lower hidden layer state;  $h_t^2$  denotes the upper hidden layer state.

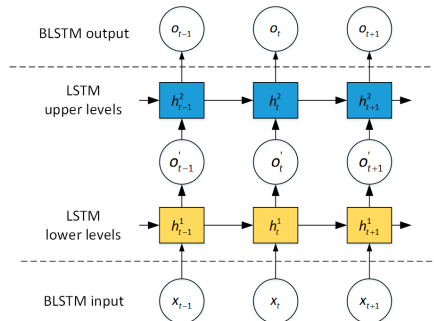


**Figure 3.** Diagram of the BLSTM scheme.

### 3.3. The RUL Prediction Algorithm's Architecture

The CNN-BLSTM fusion network model is used to predict the RUL for lithium-ion batteries, as displayed in Figure 4. The proposed model chiefly comprises the input layer, the convolutional layer, the pooling layer, the BLSTM layer, the dropout layer and the fully connected layer. The 1D CNN performs feature extraction from the time series data using the convolutional layer and diminishes the dimensionality of the input data through the max pooling layer, effectively avoiding the complexity of inputting data into the BLSTM and accelerating the training of the BLSTM network. However, the 1D CNN cannot extract the time information dependency relationship of adjacent data, BLSTM is effective in learning the coupling connection among contiguous time series data on its time axis, but it exhibits limitations in capturing deeper features and extracting information from the data. In this paper, the advantages of the 1D CNN networks and the BLSTM networks are supplemented by their integration. Each functional layer's learning process is described below.

Step 1: The data on normalized lithium-ion battery capacity is utilized as input for the whole model;

Step 2: The convolutional layer in the CNN applies a convolutional kernel to retrieve details about feature from input data, and the pooling layer retrieves feature information to minimize data dimension while maintaining essential feature details;

Step 3: The BLSTM layer computes the output data of the CNN layer using both the upper and lower LSTM hidden layers;

Step 4: In the dropout layer, the grey neural nodes do not participate in network training, which effectively alleviates the interaction between hidden layer nodes and avoids the dependence on local features during the training phase to increase the model's generalization capacity;

Step 5: Finally, the association between the output sequences of the hidden layer is extracted through the fully connected layer, and the prediction results are mapped onto the output space to complete the battery capacity based on the prediction of the multi-step.

The dropout layer has been incorporated into the model algorithm to enhance the generalization of the 1D CNN-BLSTM hybrid neural network. The dropout technique sets probability values in the neural network to deactivate some of the hidden layer nodes, as shown in Figure 4 of the dropout layer. The grey neural nodes in the dropout layer are not involved in network training, which effectively alleviates the interaction between nodes in the hidden layer, and avoids dependency on local characteristics in the training procedure. The output of the 1D CNN-BLSTM hybrid neural network without the dropout layer is shown in Equation (10), and the output of the 1D CNN-BLSTM fusion neural network with the dropout layer added is shown in Equation (14).

$$r \approx \text{Bernoulli}(p) \quad (13)$$

$$o_t = \sigma(W_o \cdot x_t + U_o \cdot h_{t-1} + b_o) \cdot r \quad (14)$$

where the dropout layer uses the *Bernoulli* function to generate a random vector  $r$  of 0 or 1 with probability  $p$  (the dropout value), thus deactivating some of the hidden layer nodes.

During the training procedure of the 1D CNN-BLSTM neural network, the network's weights and biases are updated iteratively using the Adam optimizer algorithm. The main reasons are: firstly, the momentum term and adaptive learning rate adjustment of the Adam algorithm can accelerate the convergence process of the neural network, thus reducing the training time. Secondly, the Adam algorithm usually has good stability during the training process, which can reduce the occurrence of the gradient explosion or vanishing problem and thus better maintain the numerical stability of the network.

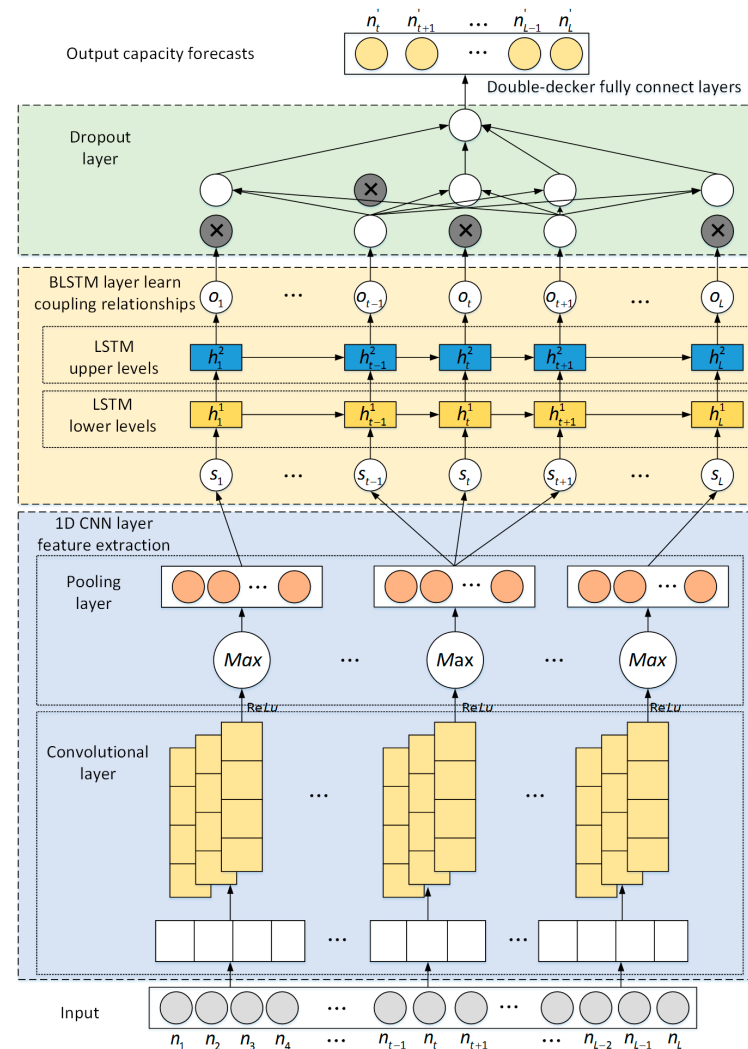


**Figure 4.** The framework diagram of the 1D CNN-BLSTM model.

The 1D CNN-BLSTM neural network establishes the mapping relationship between the early and late capacity, and makes a prediction for the unknown capacity sequence. The predicted value of capacity for every cycle following the beginning point is gained by iterative prediction, which in turn calculates the lithium-ion battery RUL. The procedures for predicting the RUL of lithium-ion batteries depend on the 1D CNN-BLSTM model, as depicted in Figure 5.

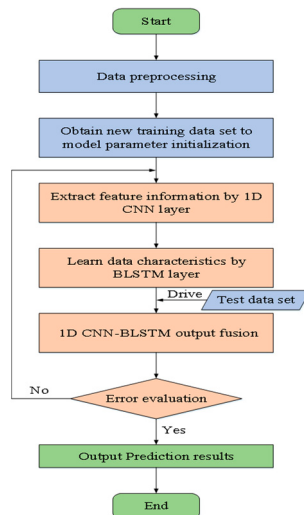


**Figure 5.** Process of training the hybrid model.

#### 4. Experiment with Prediction and Analyze the Results

In this paper, lithium-ion batteries datasets with two different electrode materials are utilized to validate the suggested algorithm's efficiency. The experimental hardware platform is based on Intel (R) Core (TM) i7-10875H CPU @ 2.30 GHz (8 cores, 16 processes) and NVIDIA GeForce RTX 2060; operating system: Windows 10 (64-bit); memory: 16 GB.

The lithium-ion battery capacity and the number of charge/discharge cycle cycles are used as input variables to the model, and the output variable is the remaining usable capacity of the battery. The dataset is divided into the training set and the test set:  $X = [X_{train}, X_{test}]$ , where  $X_{train} = [n_1, n_2, \dots, n_L]$ , and  $X_{test} = [n'_1, n'_2, \dots, n'_K]$ , in which  $L$  and  $K$  are the lengths of the training and test data, respectively.

##### 4.1. Experimental Datasets and Preprocessing

The first group experimental dataset from the NASA Prognostics Center of Excellence (PCoE) [42]. Four batteries, B5, B6, B7 and B18, were chosen as the research objects for the first group battery dataset. During the experimental data collection phase, B5 and B6 data were utilized as the training set, and B7 and B18 data were utilized as the test set, respectively, the model was trained and validated on the experimental platform. This method of dividing the dataset was chosen because the data distribution between the training and test sets can achieve a certain degree of consistency, which improves the generalization ability of the model. And it can ensure a comprehensive assessment of the model's performance at different stages to better understand the model's prediction of battery performance at different stages, rather than the prediction results at a specific point in time. Figure 6 depicts the capacity degradation curve as a function of the amount of cycles discharge from two lithium-ion batteries. Table 2 presents the specific elements of the chosen NASA lithium-ion batteries.

**Table 2.** NASA research on lithium-ion battery parameters.

Battery	Type	Rated Capacity	Experimental Cycle Number	Charge/Discharge Cut-Off Voltage
B5	18650 NMC	2 Ah	168	4.2/2.7 V
B6	18650 NMC	2 Ah	168	4.2/2.5 V
B7	18650 NMC	2 Ah	168	4.2/2.3 V
B18	18650 NMC	2 Ah	132	4.2/2.5 V

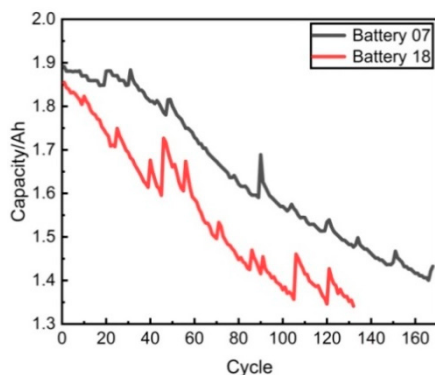


**Figure 6.** NASA battery capacity decay curve.

The second group experimental dataset was provided by CALCE at the University of Maryland [43]. This paper studies two batteries, CX2-33 and CX2-34. During the experimental data collection process, the two battery samples were split into a ratio of 8:2, using 80% of the capacity data as the training, and 20% of the remaining data for the test, and the model was trained and validated on the experimental platform. Figure 7 depicts the capacity degradation curve as a function of the amount of cycles discharge from two lithium-ion batteries. Table 3 presents the specific elements of the chosen CALCE lithium-ion batteries.

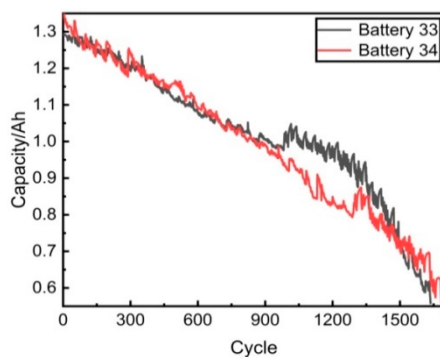


**Figure 7.** CALCE battery capacity decay curve.

**Table 3.** CALCE research on lithium-ion battery parameters.

Battery	Type	Rated Capacity	Experimental Cycle Number	Charge/Discharge Cut-Off Voltage
CX2-33	INR 18650-20R	1.35 Ah	1701	4.2/2.7 V
CX2-34	INR 18650-20R	1.35 Ah	1735	4.2/2.7 V

The aging experiment of lithium-ion batteries undergoes two dominating procedures: charging and discharging. Lithium-ion batteries are charged with a constant current of 1.5 A until the voltage reaches 4.2 V. Then, the battery continues to charge at a constant voltage of 4.2 V until the charging current drops to 20 mA. The discharge process is carried out at a constant current of 2 A until the voltage of each lithium-ion battery drops to a predetermined voltage value. Aging is carried out under different conditions based on different set values. Generally, when the actual capacity is less than 70% of the rated capacity, the “failure threshold” for battery aging is deemed to occur. Lithium-ion batteries may experience sudden fluctuations in available capacity during capacity degradation, referred to as the capacity regeneration phenomenon [44,45], which makes the prediction of battery RUL difficult.

#### 4.2. Data Normalization

The MinMaxScaler normalization process is scaling of the data features, and the MinMaxScaler normalization method transforms the interval of all retrieved eigenvalues to [0, 1] [46]. The formula is shown in (15).

$$X^* = \frac{x - x_{\min}}{x_{\max} - x_{\min}} \quad (15)$$

where  $X^*$  represents the normalization lithium-ion battery capacity data,  $x_{\max}$  and  $x_{\min}$  represents the maximum and minimum values in the lithium-ion battery capacity data samples, respectively.

#### 4.3. Metrics for Assessment

To better assess the algorithm's performance, this paper selects the root mean square error (*RMSE*), the mean absolute error (*MAE*), the R-square ( $R^2$ ) and the mean absolute percentage error (*MAPE*) as evaluation criteria to validate the effectiveness. These are defined by the following formulae.

- (1) *RMSE* denotes the normative deviation of the distinction between the observed value and the anticipated value.

$$RMSE = \sqrt{\frac{1}{n} \sum_{i=1}^n (y_i - \hat{y}_i)^2} \quad (16)$$

- (2) *MAE* denotes the average of the absolute errors between the expected values and observed values.

$$MAE = \frac{1}{n} \sum_{i=1}^n |y_i - \hat{y}_i| \quad (17)$$

- (3)  $R^2$  denotes the degree of fit between the prediction model anticipated capacity curve and the observed capacity. The value range is 0–1. The more near the value is to 1, the greater the regression fit, and vice versa.

$$R^2 = 1 - \frac{\sum_{i=1}^n (y_i - \hat{y}_i)^2}{\sum_{i=1}^n (y_i - \bar{y}_i)^2} \quad (18)$$

- (4) *MAPE* denotes a percentage representing the absolute difference between the predicted and observed value.

$$MAPE = \frac{1}{n} \sum_{i=1}^n \left| \frac{y_i - \hat{y}_i}{y_i} \right| \quad (19)$$

where  $y_i$  denotes the real capacity value,  $\hat{y}_i$  denotes the predicted capacity value, and  $\bar{y}_i$  denotes the average capacity value. The smaller the value of these three metrics, *MAPE*, *MAE* and *RMSE*, the better the prediction efficacy.

#### 4.4. Comparative Experimental Results and Analysis

We validated the relatively high accuracy and stability of the results obtained by the proposed model when employed for lithium-ion battery RUL prediction. The BP, 1D CNN, LSTM, BLSTM, 1D CNN-LSTM and 1D CNN-BLSTM model were used for experimental comparisons to predict the lifespan of the B7 and B18 batteries taken from the NASA dataset, and the CX2-33 and CX2-34 batteries taken from the CALCE dataset, respectively.

#### 4.4.1. Prediction Results Based on NASA Dataset

In this experiment, the B5 and B6 batteries were chosen as the training set, and the B7 and B18 batteries were selected as the test set, respectively, and the overall cycle time of the battery was used as the RUL prediction experiment result. Comparison of the prediction model structures is seen in Table 4, and the prediction results are displayed in Tables 5 and 6 and Figures 8 and 9.

**Table 4.** The parameters of the structure of a lithium-ion battery prediction model from the NASA dataset.

Method	The Number of Hidden Layers	Batch Size	Kernel Size	Activation Function	Dropout	Optimization Function	Learning Rate	Epochs
BP	$BP_L = 1 \& Dense_L = 2$	8	-	ReLU	0.3	Adam	0.001	150
1D CNN	$CNN_L = 1 \& Max_L = 1 \& Dense_L = 2$	8	2	ReLU	0.3	Adam	0.001	150
LSTM	$LSTM_L = 1 \& Dense_L = 2$	8	-	ReLU	0.3	Adam	0.001	150
BLSTM	$LSTM_L = 2 \& Dense_L = 2$	8	-	ReLU	0.3	Adam	0.001	150
1D CNN-LSTM	$CNN_L = 1 \& Max_L = 1 \& LSTM_L = 1 \& Dense_L = 2$	8	2	ReLU	0.3	Adam	0.001	150
1D CNN-BLSTM	$CNN_L = 1 \& Max_L = 1 \& LSTM_L = 2 \& Dense_L = 2$	8	2	ReLU	0.3	Adam	0.001	150

$BP_L$ ,  $CNN_L$ ,  $Max_L$ ,  $LSTM_L$ ,  $Dense_L$ , represent the number of BP layers, 1D convolution layers, max pooling layers, LSTM layers, and dense layers, respectively.

**Table 5.** RUL prediction errors for the B7 battery based on different models.

Battery	Model	MAE	RMSE	MAPE	R <sup>2</sup>
B7	BP	0.025	0.032	1.671	0.928
	1D CNN	0.028	0.035	1.634	0.941
	LSTM	0.018	0.024	1.076	0.971
	BLSTM	0.024	0.03	1.460	0.955
	1D CNN-LSTM	0.019	0.026	1.151	0.966
	1DCNN-BLSTM	0.013	0.018	0.804	0.983

**Table 6.** RUL prediction errors for the B18 battery based on different models.

Battery	Model	MAE	RMSE	MAPE	R <sup>2</sup>
B18	BP	0.062	0.073	1.906	0.894
	1D CNN	0.020	0.029	1.324	0.942
	LSTM	0.014	0.026	0.885	0.951
	BLSTM	0.016	0.027	1.065	0.949
	1D CNN-LSTM	0.016	0.028	1.035	0.945
	1DCNN-BLSTM	0.016	0.025	1.078	0.957

From the comparison of the results in Table 6 and Figure 9, it can be seen that the prediction evaluation index results of the BP model in B18 lithium-ion battery are poor. The BP model has low prediction accuracy and low prediction fit. The RUL prediction results of the 1D CNN model in B5 and B18 lithium-ion batteries show that the model has a good prediction fit, and the  $R^2$  value is greater than 0.94, but the RMSE and MAPE errors are

large and the prediction accuracy is low. Compared with the prediction results of the BP model, the 1D CNN model has higher prediction accuracy and fit.

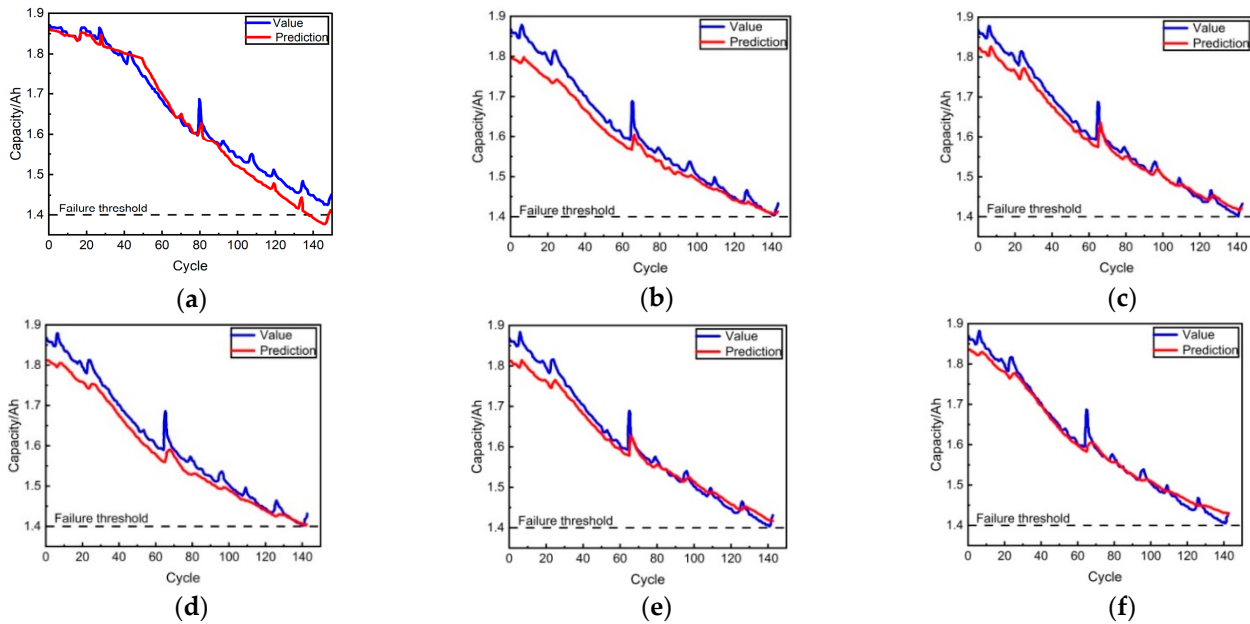


**Figure 8.** RUL prediction results of different prediction models for the B7 battery. (a) BP. (b) 1D CNN. (c) LSTM. (d) BLSTM. (e) 1D CNN-LSTM. (f) 1D CNN-BLSTM.

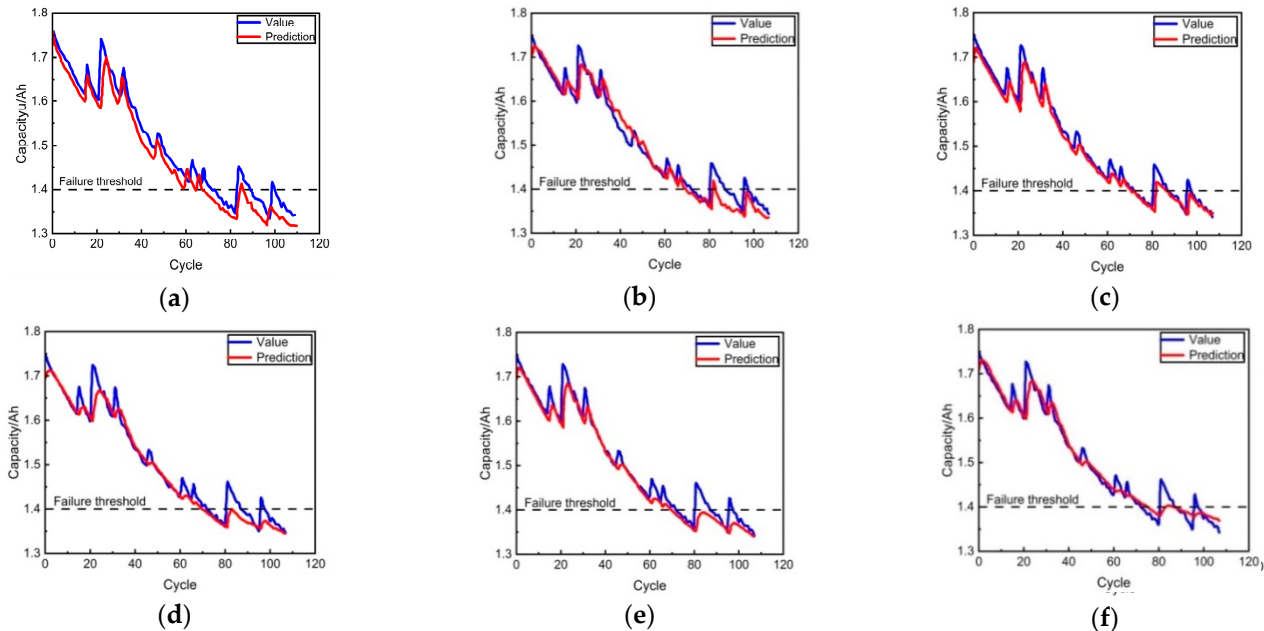


**Figure 9.** RUL prediction results of different prediction models for the B18 battery. (a) BP. (b) 1D CNN. (c) LSTM. (d) BLSTM. (e) 1D CNN-LSTM. (f) 1D CNN-BLSTM.

The 1D CNN is mainly used to explore deep aspects of data and lacks the ability of time series analysis, while LSTM and BLSTM use memory units to retain important information of input data, and have strong analysis capabilities for data with time series characteristics, but cannot explore the deep characteristics of time series. Compared with the prediction results of the 1D CNN model, the prediction error results of the LSTM model and the BLSTM model were significantly reduced on the B7 battery, with  $MAE$ ,  $RMSE$  and  $MAPE$  falling by 0.01, 0.004, 0.011, 0.005 and 0.558, 0.174, respectively, and  $R^2$  rising by

0.03, 0.014; on the B18 battery, *MAE*, *RMSE* and *MAPE* decreased by 0.006, 0.004, 0.003, 0.002 and 0.439, 0.259, respectively, and  $R^2$  rose by 0.009, 0.007. When the training data are relatively small, BLSTM tends to rely on local features of the training data. As can be seen from Tables 5 and 6, the BLSTM model has slightly larger prediction error results than that of the LSTM model. From the analysis of the total prediction results, the prediction error results of the 1D CNN, LSTM and BLSTM algorithms are large, and prediction precision is worse than that of other algorithms. The 1D CNN-LSTM integrates LSTM on the basis of 1D CNN, which combines the ability to mine deep features of data and analyze time series data to improve the prediction accuracy of 1D CNN. On the B7 battery, *MAE*, *RMSE* and *MAPE* decreased by 0.009, 0.009 and 0.483, respectively, and  $R^2$  rose by 0.015; on the B18 battery, *MAE*, *RMSE* and *MAPE* decreased by 0.004, 0.001 and 0.289 and  $R^2$  rose by 0.003. According to the four evaluation metrics, the pure LSTM algorithm is slightly better than the 1D CNN-LSTM algorithm; on the B7 battery, *MAE*, *RMSE* and *MAPE* rose by 0.001, 0.002 and 0.075, respectively, and  $R^2$  fell by 0.005; on the B18 battery, *MAE*, *RMSE* and *MAPE* rose by 0.002, 0.002 and 0.15 and  $R^2$  decreased by 0.006. The 1D CNN-LSTM fusion algorithm has good estimation performance; it still has poor accuracy, and the fitting degree and accuracy of prediction are decreased. To increase prediction accuracy and further enhance estimate performance, we employ the 1D CNN-BLSTM approach. The 1D CNN-BLSTM integrates 1D CNN on the basis of BLSTM, which combines the deep features of mining data and better learns the coupling relationship between continuous time series data on the timeline, which solves the problem that BLSTM easily relies on local features of training data when the training data are relatively small, and improves the accuracy of model prediction; on both the B7 and B18 batteries, the *MAE*, *RMSE* and *MAPE* values of the 1D CNN-BLSTM fusion algorithm are lower than those of the single algorithm, and the  $R^2$  values are higher than those of the single algorithm, which confirms that the 1D CNN-BLSTM fusion algorithm greatly improved the capacity prediction performance. In addition, the 1D CNN-BLSTM algorithm obtains *MAE*, *RMSE* and *MAPE* values with smaller prediction error results than the 1D CNN-LSTM algorithm. In the case of the B7 battery, *MAE*, *RMSE* and *MAPE* decreased by 0.006, 0.008 and 0.347, respectively.  $R^2$  increased by 0.017. In the case of the B18 battery, *MAE* remain unchanged, *RMSE* decreased by 0.003, and *MAPE* and  $R^2$  increased by 0.043 and 0.012, respectively. Based on the thorough examination of the prediction outcomes for B7 and B18 batteries, the 1D CNN-BLSTM model demonstrates superior prediction reliability and precision compared to other prediction models.

It can be seen from Figure 8 that compared with the prediction result plot of the 1D CNN model, the fit between the predicted capacity curve and the actual capacity curve of the LSTM model and the BLSTM model is significantly improved compared with the prediction result plot of the B7 battery, because the LSTM network has strong analytical ability for data with time series characteristics. It can be observed from Figure 8 that taking B7 battery for instance, the 1D CNN, LSTM and BLSTM algorithms have a good prediction effect in the latter period of battery charging and discharging, and the capacity prediction curves in the initial and intermediate phases are poorly fitted to the actual capacity curves. The LSTM and BLSTM models exhibit a point of first coincidence between the predicted capacity curves and actual capacity curves after approximately 80 and 100 cycles, respectively; while the amount of cycles in which the 1D CNN model curve's first coincide point is approximately 110, the first coincidence point among the capacity prediction curve and real capacity curve of 1D CNN model is obviously later than that of LSTM and BLSTM model. It was again verified that the LSTM model has strong analytical ability for data with time series characteristics. The fitting degree among the predicted curves and the actual curves of the LSTM and BLSTM models is improved compared with the 1D CNN model. In addition, 1D CNN-LSTM integrates LSTM on the basis of 1D CNN, and it can be seen from (b) and (e) in Figures 8 and 9 that the fit between the predicted capacity curve and the actual capacity curve of the 1D CNN-LSTM model is significantly better than that of the 1D CNN model.

Both the 1D CNN-LSTM and 1D CNN-BLSTM models are able to track the capacity degradation state of lithium-ion batteries. However, the 1D CNN-LSTM fusion model only has a single-layer LSTM layer. Compared to the double-layer LSTM layer, this fusion model has poor ability to capture the deep dependency relationship between lithium-ion battery capacity and charge discharge cycle cycles, and cannot ensure the best accuracy in tracking the degradation process, resulting in poor generalization ability. With the addition of the upper LSTM layer, the 1D CNN-BLSTM model can predict the RUL of lithium-ion batteries with an optimal model structure, and its prediction curves can better match the actual capacity curves. Using the B7 battery as an illustration, the amount of cycles whereby the predicted and actual capacity curves of the 1D CNN-LSTM model and 1D CNN-BLSTM model first coincide are approximately 70 and 30, respectively. Therefore, the 1D CNN-BLSTM model outperforms the 1D CNN-LSTM model in terms of prediction precision. Observing the five algorithm prediction curves of the B18 battery, it is characterized by large fluctuations and oscillations during the capacity drop, making it challenging to predict using these datasets. However, the 1D CNN-BLSTM generated excellent outcomes contrasted with other models. All graphs illustrate that the prediction curves of the fusion methods are most closely related to the real capacity degradation curves compared to the individual algorithms. The 1D CNN-BLSTM model outperforms the CNN, LSTM, BLSTM and 1D CNN-LSTM models in predicting the battery capacity decay trend; this demonstrates that the 1D CNN-BLSTM model is more accurate and reliable at RUL prediction.

#### 4.4.2. Prediction Results Based on the CALCE Dataset

The encouraging outcomes found in the NASA dataset were validate using the CALCE dataset. The 1D CNN-BLSTM fusion algorithm was used for the RUL prediction of CX2-33 and CX2-34. Because the two battery samples were split into an 8:2 ratio during the experimental data collection, the remaining 20% of the capacity data was chosen as the test sample. Therefore, the remaining 20% of the starting capacity data is chosen as the predicted result of the rated capacity estimate. A comparison of the prediction model structures is seen in Table 7, and the prediction findings are provided in Tables 8 and 9, as well as in Figures 10 and 11.

**Table 7.** The parameters of the structure of a lithium-ion battery prediction model from the CALCE dataset.

Method	The Number of Hidden Layers	Batch Size	Kernel Size	Activation Function	Dropout	Optimization Function	Learning Rate	Epochs
BP	$BP_L = 1 \& Dense_L = 2$	16	-	ReLU	0.3	Adam	0.0001	150
1D CNN	$CNN_L = 1 \& Max_L = 1 \& Dense_L = 2$	16	3	ReLU	0.3	Adam	0.0001	150
LSTM	$LSTM_L = 1 \& Dense_L = 2$	16	-	ReLU	0.3	Adam	0.0001	150
BLSTM	$LSTM_L = 2 \& Dense_L = 2$	16	-	ReLU	0.3	Adam	0.0001	150
1D CNN-LSTM	$CNN_L = 1 \& Max_L = 1 \& LSTM_L = 1 \& Dense_L = 2$	16	3	ReLU	0.3	Adam	0.0001	150
1D CNN-BLSTM	$CNN_L = 1 \& Max_L = 1 \& LSTM_L = 2 \& Dense_L = 2$	16	3	ReLU	0.3	Adam	0.0001	150

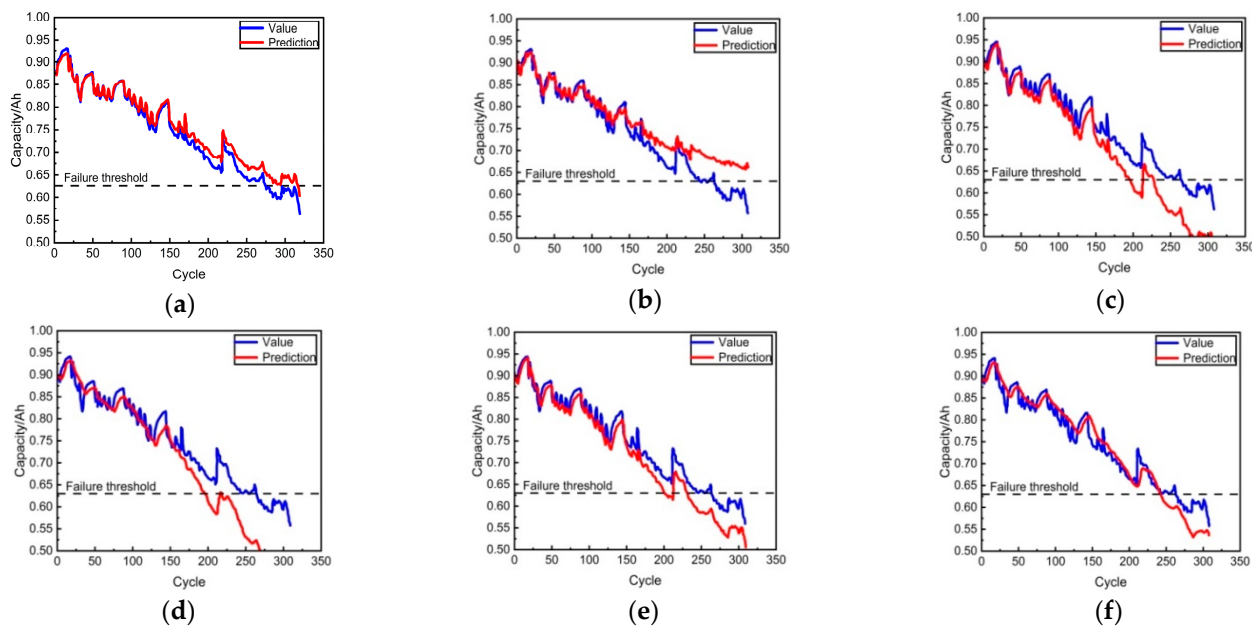
**Table 8.** RUL prediction errors for the CX2-33 battery based on different models.

Battery	Model	MAE	RMSE	MAPE	$R^2$
CX2-33	BP	0.048	0.057	6.749	0.685
	1D CNN	0.030	0.039	4.564	0.855
	LSTM	0.044	0.055	6.599	0.712
	BLSTM	0.051	0.070	7.681	0.540
	1D CNN-LSTM	0.028	0.033	4.043	0.895
	1DCNN-BLSTM	0.023	0.029	3.189	0.922

**Table 9.** RUL prediction errors for the CX2-34 battery based on different models.

Battery	Model	MAE	RMSE	MAPE	$R^2$
CX2-34	BP	0.057	0.071	7.836	0.531
	1D CNN	0.026	0.029	3.733	0.751
	LSTM	0.022	0.026	3.268	0.798
	BLSTM	0.041	0.046	6.081	0.345
	1D CNN-LSTM	0.027	0.032	4.047	0.687
	1DCNN-BLSTM	0.014	0.019	2.105	0.890

Figures 10 and 11 illustrate the exact results of the prediction for CALCE batteries, which have seen more capacity drop cycles than NASA batteries. Figures 10f and 11f illustrates this, and the 1D CNN-BLSTM model actual capacity curve and predicted capacity curve are quite similar. Therefore, the 1D CNN-BLSTM model achieves greater precision in RUL prediction and exhibits similar performance across various lithium-ion batteries, making it suitable for this task. Tables 8 and 9 show that the MAE, RMSE, and MAPE values of the 1D CNN-BLSTM fusion algorithm are lower than that of the other four algorithms and the  $R^2$  values are higher than that of the other four algorithms on both the CX2-33 and CX2-34 batteries. Tables 8 and 9 summarize RUL prediction errors values of the two cells in the CALCE datasets. The experiment clearly validates the favorable outcomes of the proposed 1D CNN-BLSTM fusion method in achieving high prediction accuracy.

**Figure 10.** RUL prediction results of different prediction models for CX2-33 battery. (a) BP. (b) 1D CNN. (c) LSTM. (d) BLSTM. (e) 1D CNN-LSTM. (f) 1D CNN-BLSTM.

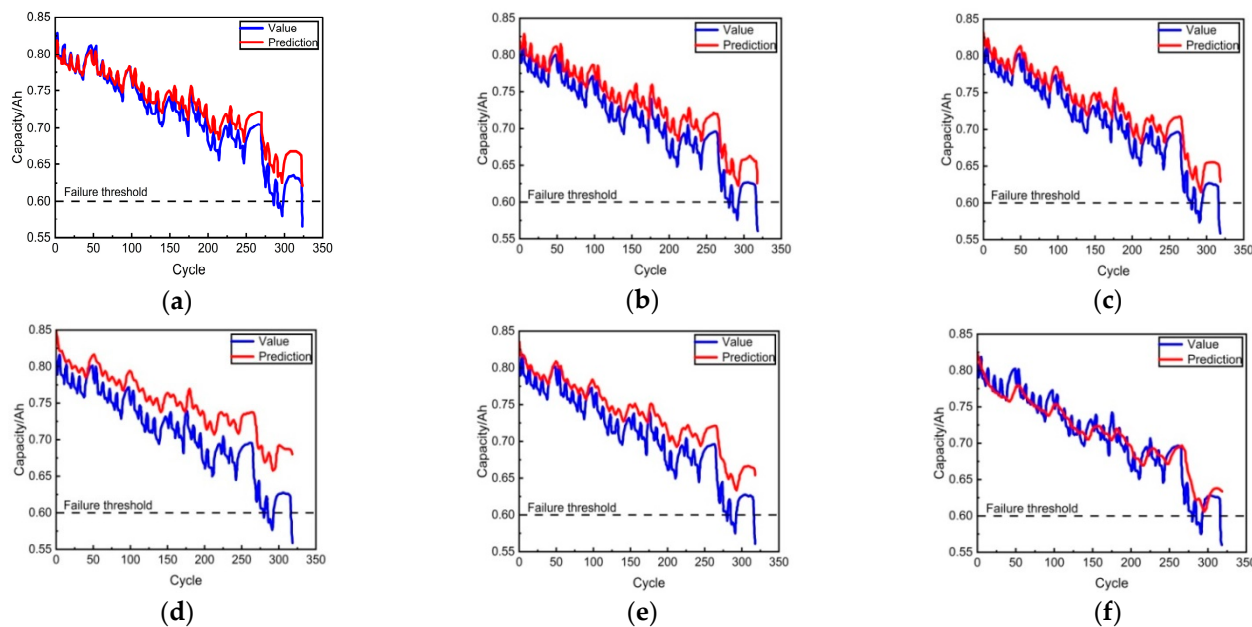


**Figure 11.** RUL prediction results of different prediction models for the CX2-34 battery. (a) BP. (b) 1D CNN. (c) LSTM. (d) BLSTM. (e) 1D CNN-LSTM. (f) 1D CNN-BLSTM.

## 5. Conclusions

Aiming at solving the problems of poor prediction precision and the reliability of conventional prediction approaches for lithium-ion battery RUL, in this paper, a 1D CNN-BLSTM neural network-based approach for predicting lithium-ion battery RUL is suggested, which innovatively integrates the 1D CNN convolution neural network with the BLSTM network, and uses the 1D CNN feature extraction function and BLSTM to learn the coupling relationship of adjacent time series on the time axis to predict the trend of lithium-ion battery capacity decay. Capacity was selected as the health factor. Based on two datasets received from NASA and CALCE with various batteries, the suggested algorithm was experimentally confirmed. The experimental results show that the RMSE values are stable between 0.018 and 0.025 and 0.019 and 0.029 in the NASA and CALCE datasets, respectively, and the 1D CNN-BLSTM fusion model improves the prediction accuracy of the proposed method compared to the BP, 1D CNN, LSTM, BLSTM, and 1D CNN-LSTM models.

In the following work, we plan to improve the proposed RUL prediction method for lithium-ion batteries to improve the prediction accuracy while saving model training time.

**Author Contributions:** Validation, C.Y.; Formal analysis, J.M. and C.Y.; Investigation, J.L.; Writing—original draft, Q.Y.; Supervision, J.M., Y.T. and Y.L. All authors have read and agreed to the published version of the manuscript.

**Funding:** This work was supported in part by the National Natural Science Foundation of China [Grant No. 5217051006], the Shandong Province Natural Science Foundation [Grant No. ZR2021ME223], the Yantai Science and Technology Planning Project [Grant No.2022GCCRC158]. The authors gratefully acknowledge the great help of the fund.

**Data Availability Statement:** Data will be made available on request. The data are not publicly available due to privacy.

**Conflicts of Interest:** Author Yuhui Liu was employed by the company Suzhou Tongyuan Software & Control Technology Co., Ltd. The remaining authors declare that the research was conducted in the absence of any commercial or financial relationships that could be construed as a potential conflict of interest.

## Abbreviations

RUL	remaining useful life
1D CNN	one-dimensional convolutional neural network
EM	electrochemical models
SEI	solid electrolyte interface
RVM	related vector machines
GPR	gaussian process regression
SVR	support vector regression
L-PEM	linear prediction error method
LSTM	long short-term memory
GA-SVR	genetic algorithm-optimized support vector regression
SOH	state of health
RMSE	root mean square error
MAPE	mean absolute percentage error
BMS	battery management systems
BLSTM	bilayer long short-term memory
ECM	equivalent circuit models
ANNs	artificial neural networks
SVM	support vector machines
GP	gaussian process
AdNN	adaptive neural network
RNN	recurrent neural network
AUKF	daptive unscented Kalman filter
EMD	empirical mode decomposition
BPNN	back-propagation neural network
MAE	mean absolute error

## References

1. Xie, Y.; He, X.; Hu, X.; Li, W.; Zhang, Y.; Liu, B.; Sun, Y. An improved resistance-based thermal model for a pouch lithium-ion battery considering heat generation of posts. *Appl. Therm. Eng.* **2020**, *164*, 114455. [[CrossRef](#)]
2. Yang, S.; Zhang, Z.; Zhang, L.; Yu, H.; Yang, K.; Liu, X. CHAIN: Cyber hierarchy and interactional network. *Etransportation* **2023**, *17*, 100256. [[CrossRef](#)]
3. Du, J.; Zhang, W.; Zhang, C.; Zhou, X. Battery remaining useful life prediction under coupling stress based on support vector regression. *Energy Procedia* **2018**, *152*, 538–543. [[CrossRef](#)]
4. Wei, M.; Gu, H.; Ye, M.; Wang, Q.; Xu, X.; Wu, C. Remaining useful life prediction of lithium-ion batteries based on Monte Carlo Dropout and gated recurrent unit. *Energy Rep.* **2021**, *7*, 2862–2871. [[CrossRef](#)]
5. Wang, D.; Yang, F.; Zhao, Y.; Tsui, K. Battery remaining useful life prediction at different discharge rates. *Microelectron. Reliab.* **2017**, *78*, 212–219. [[CrossRef](#)]
6. Zubi, G.; Dufo-Lopez, R.; Carvalho, M.; Pasaoglu, G. The lithium-ion battery: State of the art and future perspectives. *Renew. Sustain. Energy Rev.* **2018**, *89*, 292–308. [[CrossRef](#)]
7. Gao, D.; Liu, X.; Zhu, Z.; Yang, Q. A hybrid CNN-BiLSTM approach for remaining useful life prediction of EVs lithium-ion battery. *Meas. Control* **2023**, *56*, 371–383. [[CrossRef](#)]
8. Hu, X.; Xu, L.; Lin, X.; Pecht, M. Battery Lifetime Prognostics. *Joule* **2020**, *4*, 310–346. [[CrossRef](#)]
9. Deng, Z.; Yang, L.; Deng, H.; Cai, Y.; Li, D. Polynomial approximation pseudo-two-dimensional battery model for online application in embedded battery management system. *Energy* **2018**, *142*, 838–850. [[CrossRef](#)]
10. Wei, Z.; Zhao, J.; Ji, D.; Tseng, K. A multi-timescale estimator for battery state of charge and capacity dual estimation based on an online identified model. *Appl. Energy* **2017**, *204*, 1264–1274. [[CrossRef](#)]
11. Yuan, Y.; Zhang, H.; Wu, Y.; Zhu, T.; Ding, H. Bayesian learning-based model-predictive vibration control for thin-walled workpiece machining processes. *IEEE/ASME Trans. Mechatron.* **2016**, *22*, 509–520. [[CrossRef](#)]
12. Wang, W. *Prediction of Remaining Life of Lithium Battery Based on Sparse Gaussian Process Regression*; Beijing Jiaotong University: Beijing, China, 2018.
13. Singh, P.; Chen, C.; Tan, C.; Huang, S. Semi-empirical capacity fading model for SOH estimation of lithium-ion batteries. *Appl. Sci.* **2019**, *9*, 3012. [[CrossRef](#)]
14. Zhang, L.; Mu, Z.; Sun, C. Remaining useful life prediction for lithium-ion batteries based on exponential model and particle filter. *IEEE Access* **2018**, *6*, 17729–17740. [[CrossRef](#)]
15. Lyu, C.; Lai, Q.; Ge, T.; Yu, H.; Wang, L.; Ma, N. A lead-acid battery's remaining useful life prediction by using electrochemical model in the Particle Filtering framework. *Energy* **2017**, *120*, 975–984. [[CrossRef](#)]

16. Hu, X.; Li, S.; Peng, H. A comparative study of equivalent circuit models for lithium-ion batteries. *J. Power Sources* **2012**, *198*, 359–367. [CrossRef]
17. Seaman, A.; Dao, T.S.; McPhee, J. A survey of mathematics-based equivalent-circuit and electrochemical battery models for hybrid and electric vehicle simulation. *J. Power Sources* **2014**, *256*, 410–423. [CrossRef]
18. Dauga, S.; Aldaouab, I. Artificial neural network approach to improve the performance of battery and thermal storage. In *Smart Structures and NDE for Industry 4.0, Smart Cities, and Energy Systems*; SPIE: Bellingham, DC, USA, 2020.
19. Chang, Y.; Fang, H.; Zhang, Y. A new hybrid method for the prediction of the remaining useful life of a lithium-ion battery. *Appl. Energy* **2017**, *206*, 1564–1578. [CrossRef]
20. Yang, D.; Wang, Y.; Pan, R.; Chen, R.; Chen, Z. State-of-health estimation for the lithium-ion battery based on support vector regression. *Appl. Energy* **2018**, *227*, 273–283. [CrossRef]
21. Song, S.; Huang, H.; Ruan, T. Abstractive text summarization using LSTM-CNN based deep learning. *Multimed. Tools Appl.* **2019**, *78*, 857–875. [CrossRef]
22. Zhang, Y.; Xiong, R.; He, H.; Pecht, M. Long short-term memory recurrent neural network for remaining useful life prediction of lithium-ion batteries. *IEEE Trans. Veh. Technol.* **2018**, *67*, 5695–5705. [CrossRef]
23. Richardson, R.; Osborne, M.; Howey, D. Gaussian process regression for predicting battery state of health. *J. Power Sources* **2017**, *357*, 209–219. [CrossRef]
24. Wang, S.; Zhao, L.; Su, X.; Ma, P. Prognostics of lithium-ion batteries based on battery performance analysis and flexible support vector regression. *Energies* **2014**, *7*, 6492–6508. [CrossRef]
25. Song, Y.; Liu, D.; Hou, Y.; Yu, J.; Peng, Y. Satellite lithium-ion battery remaining useful life estimation with an iterative updated RVM fused with the KF algorithm. *Chin. J. Aeronaut.* **2018**, *31*, 31–40. [CrossRef]
26. Charkhgard, M.; Farrokhi, M. State-of-charge estimation for lithium-ion batteries using neural networks and EKF. *IEEE Trans. Ind. Electron.* **2010**, *57*, 4178–4187. [CrossRef]
27. Dai, H.; Zhao, G.; Lin, M.; Wu, J.; Zheng, G. A novel estimation method for the state of health of lithium-ion battery using prior knowledge-based neural network and Markov chain. *IEEE Trans. Ind. Electron.* **2018**, *66*, 7706–7716. [CrossRef]
28. Rezvani, M.; AbuAli, M.; Lee, S.; Lee, J.; Ni, J. A comparative analysis of techniques for electric vehicle battery prognostics and health management (PHM). *SAE Tech. Pap.* **2011**, *191*, 1–9.
29. Li, W.; Sengupta, N.; Dechent, P.; Howey, D.; Annaswamy, A.; Sauer, D. One-s hot battery degradation trajectory prediction with deep learning. *J. Power Sources* **2021**, *506*, 230024. [CrossRef]
30. Li, X.; Zhang, L.; Wang, Z.; Dong, P. Remaining useful life prediction for lithium-ion batteries based on a hybrid model combining the long short-term memory and Elman neural networks. *J. Energy Storage* **2019**, *21*, 510–518. [CrossRef]
31. Song, Y.; Yang, C.; Wang, T.; Liu, D.; Peng, Y. Hybrid approach of iterative updating for lithium-ion battery remaining useful life estimation. In Proceedings of the 2016 Prognostics and System Health Management Conference (PHM-Chengdu), Chengdu, China, 19–21 October 2016; IEEE: Piscataway, NJ, USA.
32. Mo, B.; Yu, J.; Tang, D.; Liu, H. A remaining useful life prediction approach for lithium-ion batteries using Kalman filter and an improved particle filter. In Proceedings of the 2016 IEEE international conference on Prognostics and Health Management (ICPHM), Ottawa, ON, Canada, 20–22 June 2016; IEEE: Piscataway, NJ, USA, 2016; pp. 1–5.
33. Xue, Z.; Zhang, Y.; Cheng, C.; Ma, G. Remaining useful life prediction of lithium-ion batteries with adaptive unscented kalman filter and optimized support vector regression. *Neurocomputing* **2020**, *376*, 95–102. [CrossRef]
34. Cao, J.; Li, Z.; Li, J. Financial time series prediction model based on CEEMDAN and LSTM. *Phys. A Stat. Mech. Its Appl.* **2019**, *519*, 127–139. [CrossRef]
35. Qu, X.; Kang, X.; Zhang, C.; Jiang, S.; Ma, X. Short-term prediction of wind power based on deep long short-term memory. In Proceedings of the 2016 IEEE PES Asia-Pacific Power and Energy Engineering Conference (APPEEC), Xi'an, China, 25–28 October 2016; IEEE: Piscataway, NJ, USA, 2016; pp. 1148–1152.
36. Jia, J.; Liang, J.; Shi, Y.; Wen, J.; Pang, X.; Zeng, J. SOH and RUL prediction of lithium-ion batteries based on Gaussian process regression with indirect health indicators. *Energies* **2020**, *13*, 375. [CrossRef]
37. Gao, D.; Liu, X.; Yang, Q. Hybrid neural network method of the lithium-ion battery remaining useful life prediction. In *Recent Advances in Sustainable Energy and Intelligent Systems. LSMS ICSEE 2021 2021. Communications in Computer and Information Science*; Springer: Singapore, 2021. [CrossRef]
38. Graves, A.; Mohamed, A.; Hinton, G. Speech recognition with deep recurrent neural networks. In Proceedings of the Ieee International Conference on Acoustics, Speech and Signal Processing, Vancouver, BC, Canada, 26–31 May 2013; IEEE: Piscataway, NJ, USA, 2013; pp. 6645–6649.
39. Gers, F.; Schmidhuber, J.; Cummins, F. Learning to forget: Continual prediction with LSTM. *Neural Comput.* **2000**, *12*, 2451–2471. [CrossRef] [PubMed]
40. Hochreiter, S.; Schmidhuber, J. Long short-term memory. *Neural Comput.* **1997**, *9*, 1735–1780. [CrossRef] [PubMed]
41. Lipton, Z.C.; Berkowitz, J.; Elkan, C. A critical review of recurrent neural networks for sequence learning. *arXiv* **2015**, arXiv:1506.00019.
42. Saha, B.; Goebel, K. *Battery Data Set. NASA Ames Prognostics Data Repository*; NASA Ames Research Center: Moffett Field, CA, USA, 2007. Available online: <http://ti.arc.nasa.gov/project/prognostic-data-repository> (accessed on 22 March 2023).

43. Pecht, M. Battery Data Set; Center for Advanced Life Cycle Engineering CALCE; University of Maryland. Available online: <https://web.calce.umd.edu/batteries/data.htm> (accessed on 22 March 2023).
44. Liu, K.; Shang, Y.; Ouyang, Q.; Widanage, W. A data-driven approach with uncertainty quantification for predicting future capacities and remaining useful life of lithium-ion battery. *IEEE Trans. Ind. Electron.* **2020**, *68*, 3170–3180. [CrossRef]
45. Xu, F.; Yang, F.; Fei, Z.; Huang, Z.; Tsui, K. Life prediction of lithium-ion batteries based on stacked denoising autoencoders. *Reliab. Eng. Syst. Saf.* **2021**, *208*, 107396. [CrossRef]
46. Mislick, G.K.; Nussbaum, D.A. *Cost Estimation: Methods and Tools*; John Wiley & Sons: Hoboken, NJ, USA, 2015.

**Disclaimer/Publisher’s Note:** The statements, opinions and data contained in all publications are solely those of the individual author(s) and contributor(s) and not of MDPI and/or the editor(s). MDPI and/or the editor(s) disclaim responsibility for any injury to people or property resulting from any ideas, methods, instructions or products referred to in the content.